CrossMark

ORIGINAL RESEARCH

Characterisation of the reaction mechanism between ammonia and formaldehyde from the topological analysis of ELF and catastrophe theory perspective

Agnieszka Ćmikiewicz[1] · Agnieszka J. Gordon[1] · Sławomir Berski[1]

Abstract A prototypical reaction between ammonia and formaldehyde has been investigated at the DFT(M06)/6-311++G(d,p) computational level using the Bonding Evolution Theory (BET). BET is a very useful tool for studying reaction mechanisms as it combines topological analysis of electron localisation function with the catastrophe theory. Each of two studied reactions: $H_2C=O + NH_3 \leftrightarrow HO–C(H_2)–NH_2$ (hemiaminal) and $HO–C(H_2)–NH_2 \leftrightarrow HN = CH_2$ (Schiff base) $+ H_2O$ consists of six steps. Formation of hemiaminal starts from a nucleophillic attack of nitrogen lone pair in NH_3 on the carbon atom in $H_2C=O$ and is subsequently followed by hydrogen transfer within the N–H·O bridge. A Schiff base is formed via the dehydration reaction of the hemiaminal, where the C–O bond is broken first, followed by hydrogen transfer towards the $[HO]^{\delta-}$ moiety, resulting in water and methanimine. The present paper focuses on differences in reaction mechanisms for the processes described above. The results have been compared to the reaction mechanism for stable hemiaminal synthesis from benzaldehyde and 4-amine-4H-1,2,4-triazole studied previously using the BET theory.

✉ Sławomir Berski
slawomir.berski@chem.uni.wroc.pl

1 Faculty of Chemistry, University of Wroclaw, F. Joliot-Curie 14, 50-383 Wroclaw, Poland

Introduction

The reaction of ammonia with formaldehyde was investigated in 1835 by Liebig [1]. Among its products were hemiaminals—molecular compounds containing amino and hydroxyl groups, bound to the same carbon. Hemiaminal is an initial product of the reaction between aldehyde or ketone and amine. Hemiaminals obtained from primary amines have been generally considered unstable [2]. In 2010, Barys et al. [3] developed a new general method for stable hemiaminals preparation. The synthesis has been performed using 4-amino-1,2,4-triazole and nitro-substituted benzaldehydes in acetonitrile [3].

Formal mechanism assumes that hemiaminal is formed during nucleophilic addition between amine and carbonyl, followed by hydrogen transfer from nitrogen to oxygen. Hemiaminal molecule can be further transformed into a Schiff base if a primary amine has been used for synthesis. In the elimination reaction, the imine (Schiff base) and water molecules are formed. An exemplary mechanism of hemaminal and Schiff base formation, which is shown in Scheme 1, suggests a dative character of the covalent nitrogen-carbon bond, $N \rightarrow C$. A hemiaminal formation is not a simultaneous process, since creation of the O–H bond is preceded by nucleophillic addition. Formation of a Schiff base and water is suggested to be concerted reaction, were the hydrogen transfer, the C–O bond breaking and formation of the double N=C bond occur simultaneously and in a single step. It is, however, worth checking the accuracy of this theoretical considerations using quantum chemical calculations and modern theory of chemical bond.

In our recent study on the reaction between benzaldehyde and 4-amine-4H-1,2,4-triazole, performed at the DFT(B3LYP)/6-311++G(d,p) level, the reaction mechanism

Springer
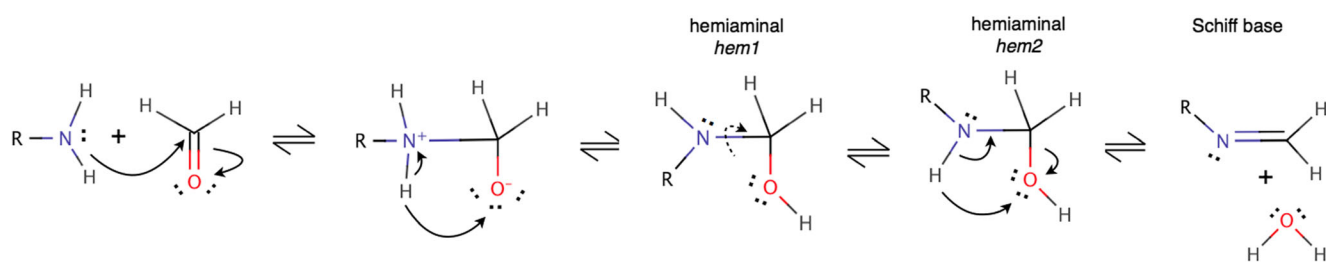
Scheme 1 General scheme of the reaction between amine and aldehyde to hemiaminal and Schiff base

has been established [4]. It, however, shows significant differences in respect to the generally assumed reaction mechanism (see Scheme 1). Scheme 2 presents a simplified picture of the chemical bond evolution in the reaction between benzaldehyde and 4-amine-4H-1,2,4-triazole. The Lewis structures and the arrows showing electron shifts have been matched to the results [4] obtained from the Bonding Evolution Theory (BET) [5] analysis. Firstly, in the reaction where hemiaminal is formed, hydrogen is transferred towards oxygen within the N–H··O bridge. Study of electronic structure, performed by means of topological analysis of electron localisation function (ELF) [6, 7], shows that after the O–H bond formation, two localisation basins, representing non-bonding electron density (formal lone pairs) on the nitrogen, $V_1(N)$ and $V_2(N)$, are present. Subsequently, those basins are combined into the single basin (lone pair) $V(N)$. Thus, the electronic structure of the amine fragment stays in agreement with the Lewis formula: there is only single lone pair on the N atom. We encourage the reader to analyse Fig. 5 in ref. [4]. In the next step, the N–C covalent bond is formed during the process of electron density donation by both atoms. In Scheme 2, two arrows show that electron densities flow from the interacting molecules towards the N···C bonding region. There is neither indication of simultaneous bond breaking nor bond formation since the respective catastrophes of ELF field are localised for different points on the intrinsic reaction coordinate (IRC) path. The second reaction is a Schiff base formation. Here, a non-simultaneous mechanism is also observed, since the C–O bond is broken first, followed by the $[OH]^{\delta-}$ formation and hydrogen transfer in the N–H··O bridge, leading to the formation of water molecule. It is worth emphasising that for the

reaction with triazole, the N–C bond is formed by electron density sharing while the formal mechanism suggests the nucleophillic attack of the amine lone pair on the carbon atom. However, it should also be remembered that stable hemiaminals, reaction products between modified benzaldehydes and 4-amine-4H-1,2,4-triazole, differ significantly from other unstable hemiaminals (Scheme 3).

The reaction between formaldehyde and ammonia has been previously studied theoretically by Williams [8] at the HF/3-21G and AM1 levels, by Hall and Smith [9] at the G2(MP2,SVP) level and by Feldmann et al. [10] at various levels of theory. The latter also determined the infinite-pressure Rice-Rampsperger-Kassel-Marcus unimolecular decomposition rate for aminomethanol water elimination. Similar study has been performed by Ding et al. [11] who investigated three different types of reactions between primary amines and variety of aldehydes (including formaldehyde) in order to describe steric and electronic inductive effects on the reaction mechanism. Erdtman et al. [12] studied reaction of methylamine with formaldehyde at the G2(MP2,SVP) level of theory.

The reaction mechanism between benzaldehyde and 4-amine-4H-1,2,4-triazole has already been proposed [4]. Similarly, a general mechanism for hemiaminal and Schiff base formation is already known. Therefore, it seems necessary to use the simplest reaction between ammonia (NH_3) and formaldehyde ($H_2C=O$), $H_2C=O + NH_3 \leftrightarrow HO–C(H_2)–NH_2 \leftrightarrow HN=CH_2 + H_2O$, to serve as a simple prototype in understanding some more complex processes. In this case, the hemiaminal, hem (aminomethanol, $HO–C(H_2)–NH_2$) and a Schiff base (methanimine, $HN=CH_2$) are formed. We will use
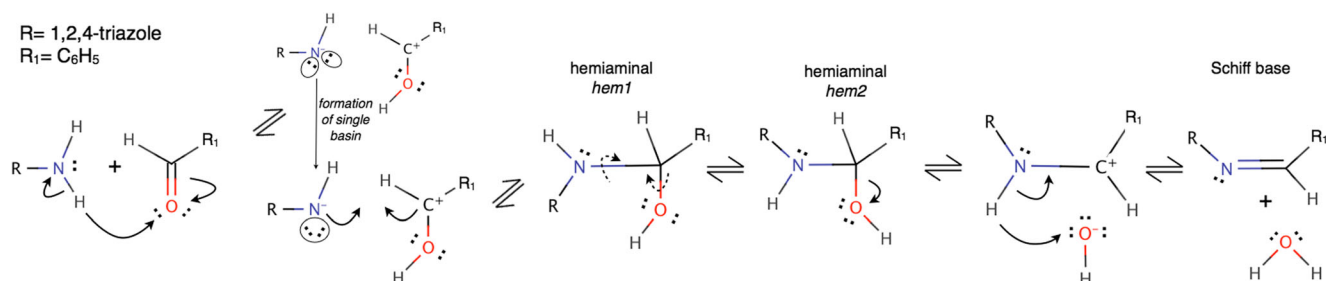
Scheme 2 Simplified representation of the reaction mechanism between benzaldehyde and 4-amine-4H-1,2,4-triazole on the basis of the BET results
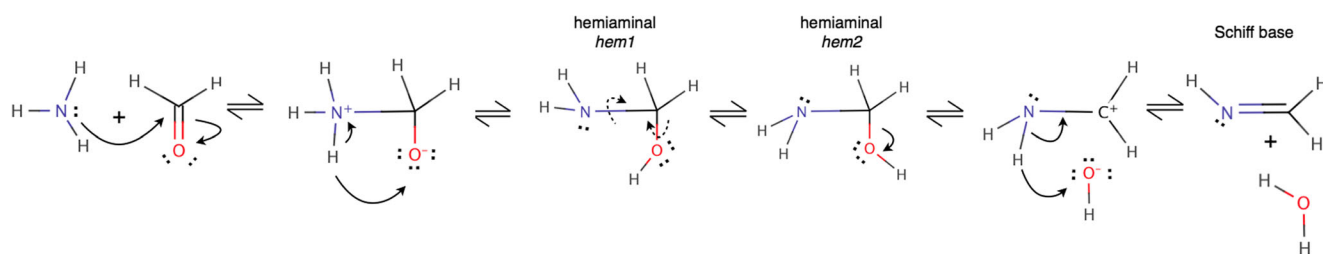
Scheme 3 Simplified representation of the reaction mechanism between ammonia and formaldehyde on the basis of the BET results

the Bonding Evolution Theory [5] as it combines topological analysis of electron localisation function (ELF) [6, 7, 13–16] with catastrophe theory [17]. ELF is one of the methods, gathered under the umbrella of quantum chemical topology [18]. The analysis has been performed in real space thus independent from the type of molecular orbital used for analysis of electronic structure. The results of BET can be presented using a slightly modified formal language of Lewis formula, generally accepted in chemistry. In our model study, the calculations have been performed for isolated molecules in the gas phase at temperature of 0 K, using DFT method.

Through our research, we are looking to answer the following:

1. What is bond breaking and bond making order in the $H_2CO + NH_3$ reaction?
2. Are there any new bonds formed in the transition states (TSs)? Are the rearrangements of chemical bonds simultaneous?
3. How does the mechanism of the reaction between H_2CO and NH_3, obtained from BET, compare to the generally known mechanism and the reaction mechanism between benzaldehyde and 4-amine-4H-1,2,4-triazole [4]?

We believe that our study will aid the understanding of reaction mechanisms in the hemiaminals and Schiff base syntheses.

Computational details

The BET analysis, including geometrical structure optimisations, relative energies and vibrational spectra, have been performed using the DFT(M06) method [19] and the 6-311++G(d,p) basis sets [20, 21] with the GAUSSIAN 09 program, G09, [22]. The optimised minima and transition states (TS1–TS3) on the potential energy surface (PES) have been confirmed by vibrational analysis. All electron density functionals used for calculation of energetic properties and presented in the Table 1 have been referenced in G09.

The reaction path has been modelled using the intrinsic reaction coordinate (IRC) introduced by Fukui [23, 24],

using CalcFC option, as it has been implemented in the G09 program. The R_x reaction coordinate has been calculated in mass-weighted steps of 0.01 bohr until the total energy minimum has been reached. The total number of points for TS1 and TS3 has been as follows: 218 (substrates), 462 and 474 (substrates), 500, respectively. For each point along the IRC path, the wave function has been obtained (approximated by a set of molecular orbitals) using the single point DFT calculations (scf=tight, NoSymm, out=wfn).

For the short (218 points) IRC path towards the NH_3 and H_2CO substrates, an additional study on the pseudo-reaction path, defined for the N–C separation, has been performed. The N–C distance, between the H_2CO and NH_3, has been scanned from 1.84 to 2.65 Å with a step of 0.05 Å, by optimising the geometrical structure for each point.

The activation energy (ΔE_a) has been calculated as a difference between total energies (E_{tot}) of the geometrical structures obtained following the IRC path towards the reagents (products) and subsequently optimised until the local minimum of total energy, E_{tot}, have been reached and of the transition structure, TS. The ΔE_a values have been corrected for the vibrational zero-point energy difference (ΔZPVE) with one imaginary frequency projected out.

For reaction 1, the interaction energy (E_{int}) is defined as a difference between E_{tot} of the reacting complex and the H_2CO and NH_3 monomers (with the geometrical structures of the complex). For reaction 2, E_{int} is a difference between E_{tot} of the post-reaction complex and the energy sum of the Schiff base and H_2O monomers (with the geometrical structures of the complex). The E_{int} values are corrected (E_{int}^{CP}) for the basis set superposition error (BSSE) using the counterpoise procedure (CP) [25] and additionally with the ΔZPVE correction ($E_{int}^{CP} + \Delta$ZPVE).

Topological analysis of the electron density, $\rho(r)$ has been performed using AIMall program [26] Topological analysis of the electron localization function has been carried out using the TopMod 09 package [27] with a cubical grid with the stepsize of 0.05 bohr. The ELF domains have been visualised using the program Chimera [28], developed by the Resource for Biocomputing, Visualisation, and Informatics at the University of California, San Francisco (supported by NIGMS P41-GM103311).

Table 1 The values of energetic parameters calculated with different DFT functionals

Functional/Param.	ΔE_s^{I}	E_{int} (I)	E_{int}^{CP} (I)	ΔE_a^{I}	ΔE_a^{II}	ΔE_a^{V}	ΔE_a^{VI}	ΔE_s^{II}	E_{int} (II)	E_{int}^{CP} (II)
APFD	− 2.81	− 4.44	− 4.03	29.32	38.64	53.76	45.22	− 5.71	− 8.00	− 7.58
B97D3	− 2.64	− 4.27	− 3.87	31.78	35.16	44.23	41.00	− 5.15	− 7.26	− 6.84
ωB97XD	− 2.55	− 4.20	− 3.83	32.65	40.05	54.54	47.38	− 5.36	− 7.55	− 7.17
B1LYP	− 4.91	− 2.95	− 2.61	38.90	40.23	50.78	46.61	− 4.50	− 6.56	− 6.18
B3LYP	− 1.57	− 3.04	− 2.67	34.16	39.17	49.58	45.22	− 4.61	− 6.69	− 6.30
CAM-B3LYP	− 2.07	− 3.59	− 3.22	32.62	40.59	53.75	46.65	− 5.38	− 7.60	−7.22
B3P86	− 1.78	− 3.40	− 2.97	28.61	38.08	52.26	43.79	− 4.88	− 7.07	− 6.66
B3PW91	− 1.15	− 2.60	− 2.17	30.19	38.25	52.33	44.94	− 4.15	− 6.25	− 5.82
BHandHLYP	− 1.92	− 3.42	− 3.09	36.77	44.52	58.68	51.57	− 4.82	− 6.99	− 6.64
BMK	− 1.31	− 6.61	− 6.30	33.60	39.50	56.01	49.15	− 4.02	− 3.15	− 2.78
PBE1PBE	− 2.17	− 3.74	− 3.32	28.44	38.66	54.43	45.09	− 5.15	− 7.32	− 6.90
PBEh1PBE	− 2.22	− 3.83	− 3.40	29.02	38.87	53.89	44.95	− 5.24	− 7.43	− 7.01
LC-ωPBE	− 1.67	− 3.08	− 2.76	30.11	41.05	59.09	48.14	− 4.75	− 6.86	− 6.48
TPSS	− 1.08	− 3.47	− 3.02	28.71	34.63	45.58	39.65	− 4.84	− 6.98	− 6.51
TPSSh	− 1.78	− 3.36	− 2.94	30.21	36.60	49.27	42.39	− 4.79	− 6.91	− 6.45
M06	− 2.66	− 4.47	− 4.00	33.21	39.52	53.28	46.63	− 5.21	− 7.50	− 7.09
M062x	−2.93	−4.59	−4.16	32.00	41.25	58.46	50.47	−5.45	− 7.82	− 7.43
M11	−2.60	−4.22	−3.79	32.06	40.20	54.83	47.67	−5.55	− 8.00	− 7.53
N12SX	−2.10	−3.72	−3.31	28.29	39.81	55.74	45.15	−5.28	− 7.48	− 7.04
MN12SX	−2.57	−4.16	−3.70	32.12	40.14	55.83	48.90	−4.60	− 6.80	− 6.29

Results and discussion

### Geometrical structures and energetics

The reaction between ammonia and formaldehyde (see Fig. 1) in the gas phase (vacuum, 0 K) proceeds through four local minima on the potential energy surface (PES). The mechanism shows three transition structures (TS1–3). Initially, the pre-reaction molecular complex, $H_3N\cdots C(H_2)=O$, is formed. Subsequently the complex evolves over the TS1 to aminomethanol, $H_2N–C(H_2)OH$, (hemiaminal, hem1) formally via the nucleophilic attack of the nitrogen lone pair on the carbon atom and subsequently hydrogen transfer from ammonia to oxygen from formaldehyde. As a result, two new covalent bonds, O–H and N–C, are formed. Conformational change that occurs in the hem1 molecule is associated with TS2 (hem1 ↔ hem2). The lone pair on the oxygen atom assumes the position facilitating internal transfer of the hydrogen from the − NH₂ fragment to the − OH group. In the second step, characterised by the TS3, the C–O bond is broken. This process is associated with internal transfer of hydrogen towards oxygen. This causes transformation of aminomethanol (hemiaminal, hem2) into water and methanimine, $H_2C=NH$ (Schiff base). After dehydratation, the H_2O molecule forms a post-reaction molecular complex with the methanimine ($H_2O\cdots HN=CH_2$), stabilised by the O–H⋯N hydrogen bond. Geometrical structures, optimised for the TSs and the minima on the PES calculated at the DFT(M06)/6-311++G(d,p) level are shown in Fig. 1.

Energy parameters characterising all the reactions, i.e. the energy of stabilisation, ΔE_s, the interaction energies, E_{int}, E_{int}^{CP}, for the $H_3N\cdots C(H_2)=O$ and $H_2O\cdots HN=CH_2$ complexes and the activation energies, $\Delta E_a^{I\text{-}VI}$, associated with TS1 and TS3 are collected in Table 1. Small values of $\Delta E_a^{III,IV}$ related to the conformational change hem1 ↔ hem2 (TS2) have been omitted. In order to check the effect of the DFT functional on those values, 20 different functionals have been used. The value of E_{int}^{CP} for the $H_3N\cdots C(H_2)=O$ complex is between − 2.17 kcal/mol (B3PW91) and − 6.30 kcal/mol (BMK), and that of the final $H_2O\cdots HN=CH_2$ complex are between − 2.78 (BMK) and − 7.58 kcal/mol (APFD). It is worth noting that the value of the E_{int}^{CP} can show discrepancy of up to about 290% in extreme cases (for both complexes). At the activation barrier, energy (ΔE_a^{I}) needed to form the hem1 molecule ranges between 28.29 (N12SX) and 38.90 (B1LYP) kcal/mol and is much smaller than the energy (ΔE_a^{V}) of 44.23 (B97D3)–59.09 kcal/mol (LC- ωPBE) required to form a Schiff base in the second reaction. Further details of the reaction's energy parameters are presented in Table 1.

The reliable reaction modelling has to account for the environmental effects, i.e. surrounding solvent molecules or other reacting molecules. We have performed the calculations including up to three H_2O and NH_3 molecules for the TS1

Fig. 1 Schematic energy profile of the hemiaminal and Schiff base formation from ammonia and formaldehyde
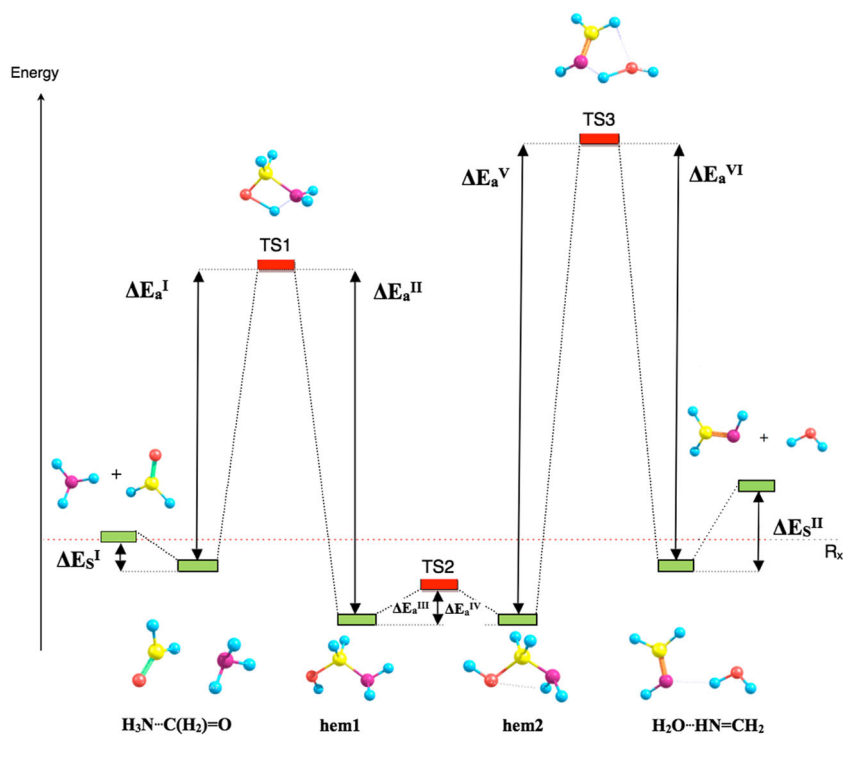
and one H_2O and NH_3 molecule for the TS3. Subsequent addition of water molecules results in decrease of the ΔE_a^{I} activation energy to 16.05, 6.09 and 6.03 kcal/mol, respectively. The ΔE_a^{II} activation energy decreases to 22.95, 18.31 and 15.46 kcal/mol, respectively. Thus, the energetic barrier needed for the reaction is essentially reduced in water environment. Similar effect occurs with ammonia, where the ΔE_a^{I} activation energy is reduced to 19.69, 15.15 and 5.74 kcal/mol, respectively. The ΔE_a^{II} is lowered to 27.13, 23.47 and 21.16 kcal/mol, respectively. In the case of the ΔE_a^{V} and ΔE_a^{VI} activation energies, related to the formation of Schiff base, the decrease in activation energy observed after adding solvent molecules is negligible. One H_2O molecule reduces these energies to 53.36 and 47.40 kcal/mol, respectively. Ammonia shows decrease to 53.80 and 46.86 kcal/mol, respectively.

Reaction mechanism obtained by bonding evolution theory (BET)

The reaction between ammonia (NH_3) and formaldehyde (H_2CO) has been investigated at the DFT(M06)/6-311++ G(d,p) computational level. For each point on the IRC path, topological analysis of ELF function has been performed. Comparison of the electronic structure between two consecutive points on the IRC path, represented by the core C(A) and valence attractors, V(A,B) and V(A), enables localisation of the catastrophes on the ELF field. Each catastrophe separates two consecutive steps of studied reactions. From a chemical

point of view, the most interesting are catastrophes associated with annihilation and creation of the valence attractors (local maxima of ELF) since they correspond to annihilation and creation of chemical bonds, V(A,B) and lone pairs, V(A). Thus, one can observe evolution of the chemical bonds, A–B, as they are broken or formed, along the reaction path (IRC). Hydrogen transfer is an exception since the proton bearing some electron density is described by the asynaptic attractor V(H) [29]. To aid better understanding of the methodology used here, the reader is encouraged to familiarise themselves with the papers published by Silvi's group [30–35]. Particularly those describing the BET theory [5] and BET applications for reaction mechanisms such as isomerisation in XNO (X=H, Cl) [36], hydrogen transfer in $H_5O_2^+$ [33], in malonaldehyde [37], in the HF–(OH)$^-$ and HCl–(OH)$^-$ complexes [38], electron transfer in the Li + Cl_2 system [39], and reaction between butadiene and ethylene [40].

A good starting point for the reaction mechanism study is the electronic structure of the weak complex $H_3N\cdots C(H_2)=O$, optimised at the last point on the IRC path, going towards ammonia and formaldehyde. Stabilisation of the complex by weak forces does not change the ELF topology of interacting molecules. The topology of ELF, observed for the isolated NH_3 and H_2CO molecules, is also observed for the complex. The number of synaptic core and valence attractors (13) is the same for isolated molecules and the complex. Such additivity of the topologies can be a consequence of a relatively large distance between the N and C atoms (2.739 Å) and weak mutual perturbation of the subsystems.

The ELF localisation domains and basin population values, $\overline{N}$, for $H_3N^{...}C(H_2)=O$ are shown in Fig. 2. The formaldehyde consists of the oxygen and carbon atomic cores, C(O) and C(C), two lone pairs localised on the oxygen atom, $V_{i=1,2}(O)$ and two $V_{i=1,2}(C,O)$ basins, characterising formally double bond, C=O. Population of each $V_{i=1,2}(C,O)$ basin is 1.16e (see Table 2), thus the formal bond order is two and differs essentially from the topological bond order, which is about 1.2. The remainder of the electron density is found in two oxygen lone pairs ($2 \times 2.61e$) and two C-H bonds ($2 \times 2.14e$). It is evident that the bond has a large contribution of the ionic character (mainly C^+O^-). In the electronic structure of ammonia one lone pair, $V_1(N)$, can be found on the nitrogen atom, with population of 2.10e and three protonated disynaptic attractors V(H1,N), V(H2,N), V(H3,N) with the basin population of 1.92e, corresponding to three N–H bonds. The ELF localisation domains presented in Fig. 2 show that the lone pair of nitrogen $V_1(N)$ is directed towards the carbon core, C(C), thus the stabilising $N^{...}C$ interaction is expected. Topological analysis of $\rho(r)$ field supports such interaction since the $(3, -1)$ critical point, CP, is localised on the atomic interaction line joining the N and C nuclei. The values of $\rho_{(3,-1)}(r) = 0.015e/bohr^3$ and $\nabla^2\rho_{(3,-1)}(r) = +0.049e/bohr^5$ confirm a non-covalent interaction. Topological analysis of ELF clearly shows that the valence basin of nitrogen, $V_1(N)$, corresponding to the lone pair in formal Lewis formula of ammonia, is of a monosynaptic type. Thus there is no covalent interaction with the C atom.

Topology of ELF obtained for the isolated NH_3 and H_2CO molecules and the $H_3N^{...}C(H_2)=O$ complex (13 core and valence attractors) describe the electronic structure of the interacting molecules in the step I of the reaction. Unfortunately, due to the limitations of the IRC procedure, the relevant points on the IRC path have not been observed.

First point on the IRC path, calculated for $R_x = -2.244$ bohr and the corresponding value of the $r(N^{...}C)$ distance, 1.846 Å, is much shorter ($\Delta r = 0.892$ Å) than that calculated for the $H_3N^{...}C(H_2) = O$ complex. Since a number of attractors for the reacting system decreases to 12, changes in topology of ELF are inevitable. Two important changes of the ELF field have been found. Firstly, in the C=O region, only one V(C,O) attractor has been observed. Secondly, in the $N^{...}C$ region, the attractor $V_1(N)$ of the monosynaptic type, characterising the non-bonding electron density on the N atom (the lone pair) in NH_3 molecule, changed from synaptic to disynaptic type, V(N,C). Thus the V(N,C) basin shares the surface with both the C(C) and C(N) core basins. According to the work of Krokidis et all [5] focused on dissociation of $H_3N–BH_3$, the V(N,C) basin suggests creation of the covalent-dative (formal) $N \rightarrow C$ bond. However, this conclusion has been drawn for much longer distances than those covered by the IRC path. Conversion of the $V_1(N)$ basin into the V(N,C) basin and reduction of the $V_{i=1,2}(C,O)$ basin into the V(C,O) basin should be observed for the points before $R_x = -2.244$ bohr.
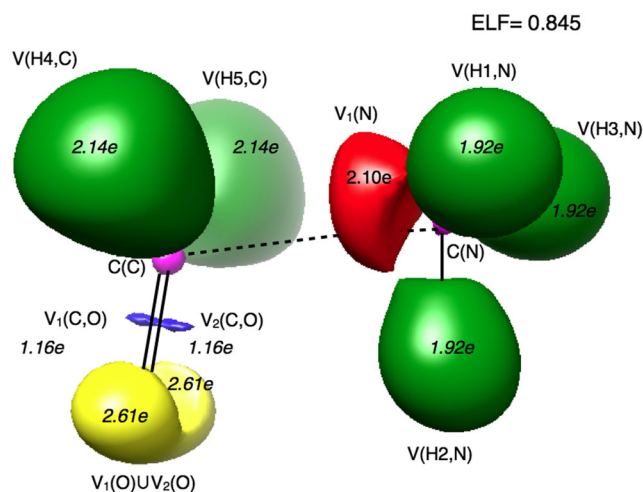
Fig. 2 ELF localisation domains for the optimised structure of the $NH_3^{...}CH_2(=O)$ complex

Analysis of the pseudo-reaction path, calculated for the $N^{...}C$ distance (see 'Computational details') shows that two $V_{i=1,2}(C,O)$ attractors and basins are annihilated and a single attractor V(C,O) is created in the cusp catastrophe for $r(N^{...}C) \approx 2.3$ Å and $r(C–O) \approx 1.2$ Å. Change of the synapticity $V_1(N)$ into V(N,C) occurs for $r(N^{...}C) \approx 1.93$ Å. Those two topological changes characterise the electronic structure of the reacting $H_3N^{...}C(H_2)=O$ complex in steps II and III, respectively.

It is worth noting that the ELF topological description of annihilation or creation of the covalent-dative bond (N–C, N–B) is complicated [5] The relevant fold catastrophe, studied by Krokidis et al. [5] for the N–B bond breaking in the $H_3N–BH_3$ molecule and associated with the V(N) to V(B,N) change ($r(B^{...}N) = 2.87$ Å) does not involve any attractor of ELF field but the repellor, $(3,+3)$ and $(3,+1)$ critical points. Full topological analysis of this type, with all the CPs thoroughly analysed, is outside the scope of our research.

All the points on the IRC path, corresponding to geometrical structures with the $r(N^{...}C)$ distance larger than 1.583 Å ($R_x = -0.104$ bohr), belong to the step III of the reaction. Total number of the core and valence attractors is 12. The mutual approach of the NH_3 and H_2CO molecules shows gradual flow of the electron density from the lone pair on N to the N-H bond in ammonia and to the $V_{i=1,2}(O)$ basins in formaldehyde (see Table 2). Such interpretation is also supported by the Mulliken charges for the C and O atoms rising from -0.007 and $-0.458e$ for $R_x = -2.244$ bohr to -0.100 and $-0.562e$ for $R_x = -0.115$ bohr. Modified Lewis structures sketched on the basis of the ELF analysis for all the points in steps I, II and III are shown in Fig. 3. The IRC path with the points grouped to different steps are shown in Fig. 4.

The first catastrophe of ELF, determining the step IV of the reaction, is observed for $R_x = -0.104$ bohr in the valence shell of the O atom in the $O^{...}H$ region for $r(O–H2) = 1.483$ Å, r(N–

Table 2 The values of the basin population (in e) for different steps of the reaction between the ammonia and formaldehyde

| Step:			I	II[a]	III[a]	IV	V	V	VI	VI	VI	VI	VII	VIII	VIII	IX	X	XI	XI		
Basin	H2CO	NH3	complex					TS1		hem1	TS2	hem2			TS3				complex	H2CNH	H2O
C(N)	–	2.11	2.11	2.11	2.11	2.11	2.11	2.11	2.11	2.11	2.11	2.11	2.11	2.11	2.11	2.11	2.11	2.10	2.10	2.11	–
C(C)	2.09	–	2.09	2.09	2.09	2.09	2.09	2.09	2.09	2.09	2.09	2.09	2.09	2.09	2.09	2.09	2.09	2.09	2.09	2.09	–
C(O)	2.12	–	2.12	2.12	2.12	2.12	2.12	2.12	2.12	2.12	2.12	2.12	2.12	2.12	2.12	2.12	2.12	2.12	2.12	–	2.12
V(H1,N)	–	1.92	1.92	1.92	1.95	2.04	2.04	2.04	2.03	2.01	1.97	1.96	1.96	1.95	1.95	1.96	1.96	1.95	1.96	1.94	–
V(H2)	–	–	–	–	–	–	0.59	0.43	–	–	–	–	–	–	–	–	–	–	–	–	–
V(H2,O)	–	–	–	–	–	–	–	–	1.47	1.71	1.71	1.71	1.71	1.72	1.73	1.74	1.74	1.70	1.68	–	1.68
V(H2,N)	–	1.92	1.92	1.94	1.97	2.11	–	–	–	–	–	–	–	–	–	–	–	–	–	–	–
V(H3,N)	–	1.92	1.92	1.94	1.97	2.04	2.03	2.04	2.04	1.98	1.96	1.96	1.87	–	–	–	–	–	–	–	–
V(H3)	–	–	–	–	–	–	–	–	–	–	–	–	–	0.48	0.48	0.39	0.39	–	–	–	–
V(H3,O)	–	–	–	–	–	–	–	–	–	–	–	–	–	–	–	–	–	1.72	1.69	–	1.68
V(H4,C)	2.14	–	2.14	2.15	2.16	2.14	2.14	2.13	2.13	2.09	2.10	2.09	2.14	2.16	2.17	2.17	2.17	2.15	2.12	2.12	–
V(H5,C)	2.14	–	2.14	2.15	2.16	2.14	2.14	2.13	2.13	2.09	2.08	2.09	2.14	2.16	2.18	2.17	2.15	2.13	2.12	2.12	–
V1(N)	–	2.13	2.10	1.97	–	–	–	–	–	–	–	–	–	–	–	–	–	–	–	–	–
V2(N)	–	–	–	–	–	–	1.53	1.72	1.96	2.06	2.16	2.10	2.11	2.30	2.43	3.44	3.29	2.93	2.64	2.68	–
V3(N)	–	–	–	–	–	–	–	–	–	–	–	–	–	1.12	1.03	–	–	–	–	–	–
V1(N,C)	–	–	–	–	1.83	1.67	1.67	1.67	1.61	1.72	1.72	1.78	1.88	2.04	2.10	2.13	}2.32	1.42	1.46	1.45	–
V2(N,C)	–	–	–	–	–	–	–	–	–	–	–	–	–	–	–	–		1.47	1.47	1.48	–
V1(C,O)	1.19	–	1.16	}2.20	}2.08	}1.47	}1.46	}1.45	}1.38	}1.30	}1.29	}1.25	–	–	–	–	–	–	–	–	–
V2(C,O)	1.19	–	1.16										–	–	–	–	–	–	–	–	–
V1(O)	2.57	–	2.61	2.69	2.78	2.88	2.84	2.76	2.47	2.31	2.37	2.37	2.49	2.11	1.86	1.77	–	–	–	–	–
V2(O)	2.57	–	2.61	2.69	2.78	2.87	2.84	2.75	2.47	2.37	2.31	2.36	2.63	2.87	2.89	2.89	2.80	2.43	2.26	–	2.25
V3(O)	–	–	–	–	–	0.31	0.37	0.54	–	–	–	–	–	–	–	–	–	–	–	–	–
V4(O)	–	–	–	–	–	–	–	–	–	–	–	–	0.75	0.77	0.95	1.02	1.48	1.97	2.26	–	2.25

[a] The points characterised for pseudo-reaction path
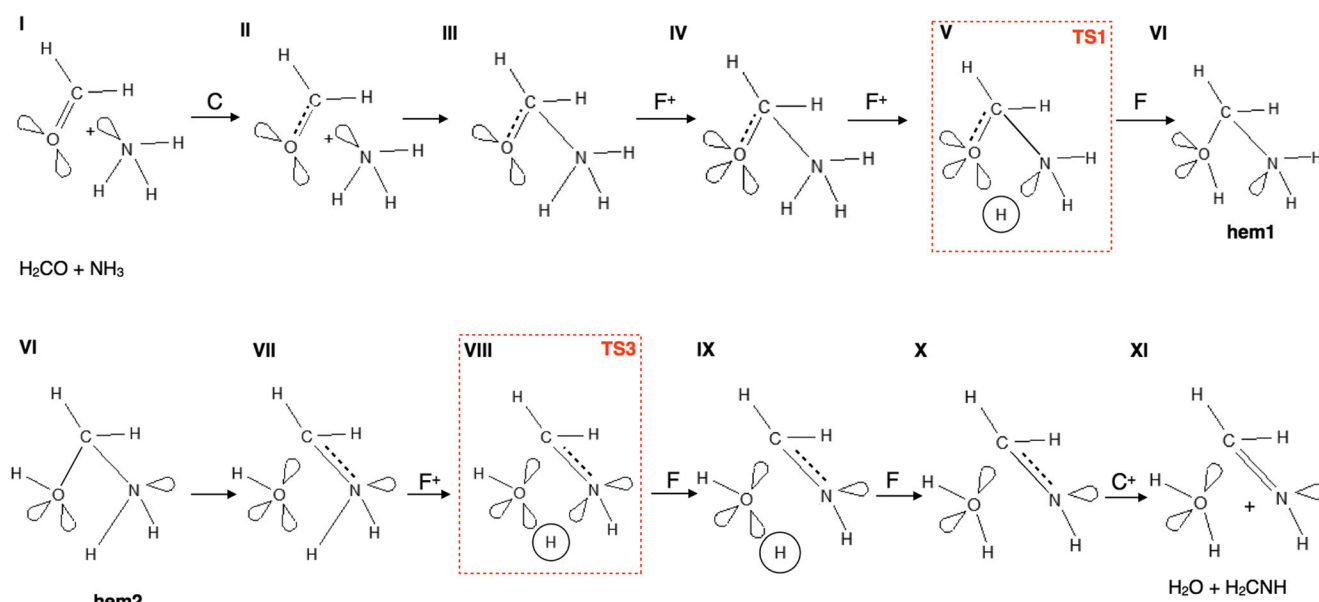
Fig. 3 Modified Lewis structures, representing evolution of the chemical bonds and lone pairs (non-bonding regions), for steps I–XI of the reaction between ammonia and formaldehyde

H2) = 1.141 Å and r(N–C) = 1.583 Å. Rehybridization of atomic orbitals on the O atom to sp³ and localisation of electron density in the O⋯H region is manifested by formation of the third region of non-bonding electron density on the O atom, represented by the V_3(O) attractor and its basin (lone pair). The number of attractors increases to 13. In the fold catastrophe (F^+), the V_3(O) attractor and critical point (3, −1) are formed. Basin population of the V_3(O) basin is 0.31e. This value is much smaller than about 2.9e of two lone pairs $V_{i=1,2}$(O). It is worth noting that localisation of the V_3(O) lone pair is associated with the transfer of the H2 atom. This step

on the IRC path is very short since the ELF topology described above is observed only for three points of the IRC path.

In step V, the N–H2 bond in ammonia, represented by the protonated attractor and basin V(H2,N), is broken. The fold catastrophe (F^+) is observed in the region of the N–H2 bond for R_x = − 0.073 bohr. Optimised parameters for this reaction are as follows: r(O–H2) = 1.467 Å, r(N–H2) = 1.153 Å and r(N–C) = 1.581 Å. Electronic structure of the broken bond consists of the proton surrounded by electron density, known as 'dressed proton', V(H2) and the region of non-bonding electron density in the vicinity of the N atom, represented by

Fig. 4 Evolution of the total energy for hemiaminal formation (reaction I) as function of the IRC coordinate with marked positions of the catastrophes on the ELF field
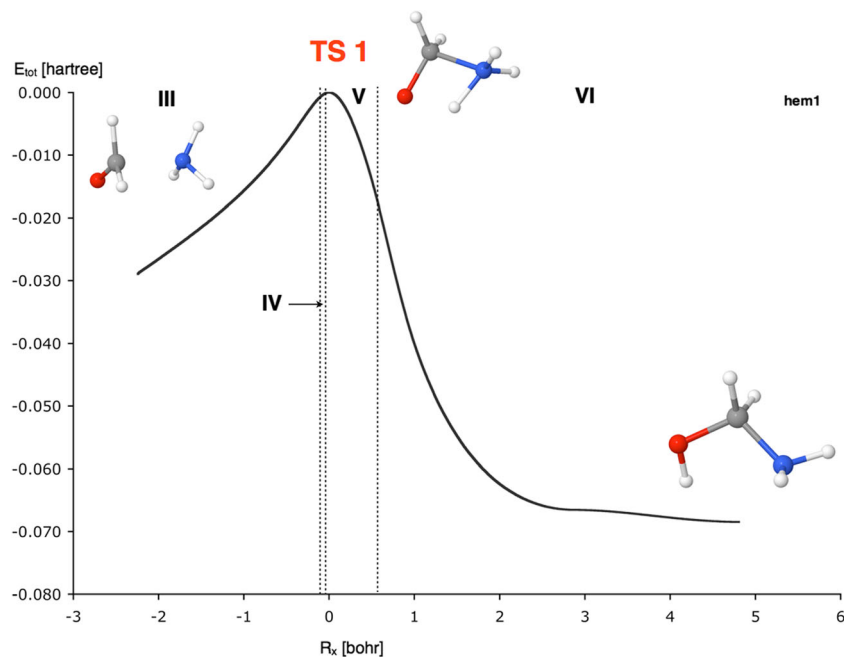
the non-bonding attractor and basin, $V_2(N)$. The number of core and valence attractors increases to 14. The NH_2 fragment consists now of two N–H bonds (N–H1, N–H3) and one region of the non-bonding electron density. The basin population of the dressed proton is 0.59e and that of the $V_2(N)$ basin is 1.53e. The same ELF topology is also observed for the electronic structure of the molecules in the TS1 (see Fig. 5), where slightly smaller basin population of V(H2) can be found (0.43e).

The final stage of hydrogen transfer in the N⋯H2⋯O bridge is observed in step VI. In effect, the O–H2 bond is created out of the non-bonding basin $V_3(O)$ and the dressed proton V(H2) basin. In the fold catastrophe (F), observed for the $R_x = 0.605$ bohr, the $V_3(O)$ attractor and the (3, −1) CP are annihilated, and a new non-critical point (CP) is created. The number of attractors decreases to 13. The catastrophe is found for the following distances: $r(O–H2) = 1.129$ Å, $r(N–H2) = 1.442$ Å and $r(N–C) = 1.561$ Å. An attractor is localised at the proton and its basin is now the disynaptic protonated basin, V(H2,O). From ELF topological point of view, the O–H2 bond has been formed. The basin population of V(H2,O) is 1.47e, but the basin is not yet 'saturated' with electron density. The final value of $\overline{N}$ obtained for the optimised geometrical structure of the hem1 is 1.71e. Comparison of the basin population evolution of previous steps shows that the V(H2,O) basin is 'filled' with electron density, coming mainly from the surrounding $V_{i=1,2}(O)$ and V(C,O) basins. Step VI also terminates the first reaction since all the chemical bonds of the hem1 are formed at this stage.

The final product of the first reaction, aminomethanol consists of the C–O bond with 1.30e, the N–C bond with 1.72e and five bonds related to the H atoms (N–H, H–C, O–H) with the basin populations in a range of 1.71–2.09e. Population of the formal single C–O bond is 1.08e smaller than a formally double C=O bond in formaldehyde (2.38e). Analysis of atomic contributions, using the procedure described by Raub and Jansen [41], shows that the C–O bond is polarised towards oxygen, donating 1.0e to the bond, while 0.3e comes from the C atom. The polarity index p_{OC} is 0.54. The covalent N–C bond with the p_{NC} index 0.35, is less heteropolar than the C–O bond. The bond is polarised towards the nitrogen as the nitrogen atom donates 1.16e and the carbon atom 0.56e. The geometrical structure of hem1, optimised to the energy minimum is also observed in the step VI of the reaction.

Reorientation of the N–H and O–H bonds in aminomethanol (hem1 ↔ hem2) is characterised by the TS2. Topological analysis of ELF shows that this step is not associated with any catastrophe. Neither rearrangement in the bond electronic structure nor lone pairs in both conformers are observed; therefore, the electronic structure of hem2—from ELF topological perspective—is the same as described for the step VI of the reaction. No further discussion for the hem1 ↔ hem2 process is deemed necessary. Values of the

basin population for hem1 and hem2 can be analysed further using data presented in Table 2.

The second reaction, where the molecular complex of the methanimine (Schiff base) with water is formed from hem2 has been analysed starting from the point on the IRC path at $R_x = −4.985$ bohr (step VI). The $r(C–O)$ value at this point is 1.423 Å. The IRC path with the points grouped to different steps are shown in Fig. 6.

At first, the C–O bond breaking is observed (step VII). It is topologically characterised by a change of the disynaptic basin V(C,O) into the monosynaptic basin V(O). This is caused by the C–O bond elongation and the transfer of the electron density mainly towards more electronegative oxygen atom. As a result, three regions of non-bonding electron density (lone pairs), $V_{i=1,2,4}(O)$ are observed in the valence shell of oxygen (sp^3 hybridisation). Consequently, the $[HO]^{\delta−}$ fragment is no longer bound to the $[H_2C–NH_2]^{\delta+}$ moiety. Since no bonding basins containing shared electron density from both molecules are present, the value of the ELF topological δ charge can be calculated as 0.7e. The number of attractors remains unchanged—13.

Topological characterisation of C–O bond breaking process is complicated, due to difficulty in pinpointing where the V(C,O) basin is transformed into V(O) on the IRC path. Such process can be associated with oscillation of the local maximum of ELF between the C(O) and C(C) cores, manifesting in change between the V(C) and V(O) types, observed on the IRC path close to the point of catastrophe. Similar difficulties have been reported before [42]. It is worth mentioning that not every C–O bond breaking is characterised by change in a synaptic basin. For example, the study on the reaction between benzaldehyde and 4-amine-4H-1,2,4-triazole [4] has shown that the C–O bond is broken through separation of the V(C,O) basin into two V(C) and V(O) monosynaptic basins. Such mechanism of bond breaking is typical for covalent bonds, while transformation of V(C,O) into V(O) indicates a presence of the dative bond (see study by Krokidis et al. [5]). In this study, the V(C,O) basin is no longer observed from $R_x = −1.25$ bohr onwards. This corresponds to the following bond lengths: $r(C–O) = 1.77$ Å, $r(O–H3) = 1.81$ Å, $r(H3–N) = 1.04$ Å. Population of the monosynaptic, non-bonding basin $V_4(O)$ is 0.75e, which is much smaller than the population of the two lone pairs $V_{i=1,2}(O)$ of 5.12e.

In the next three steps, VIII, IX, and X, hydrogen transfer in the N–H3⋯O bridge is observed, followed by water elimination. This process is similar to the H2 atom transfer in the N–H2⋯O bridge, observed for the first reaction. Elongation of the N–H3 bond causes electron density redistribution towards the H3 and N atoms. As a result, new local maximum $V_3(N)$ appears in the vicinity of the N atom in the fold catastrophe (F^+). This catastrophe begins step VIII of the reaction. The number of the core and valence attractors increases to 14. The catastrophe is found before the TS3 for $R_x = −0.189$ bohr, corresponding to $r(C–$

Fig. 5 The core and valence
attractors and ELF localisation
domains for the transition
structure TS1 for the hemiaminal
formation reaction
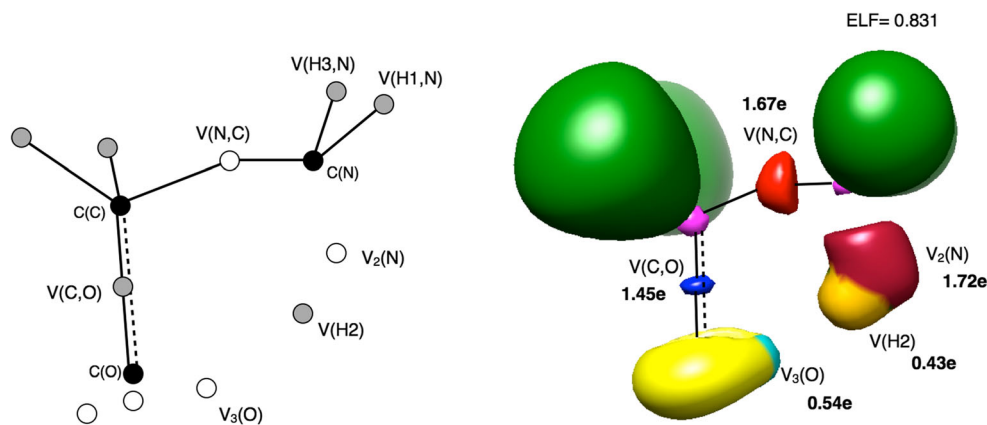
O) = 1.861 Å, r(O–H3) = 1.385 Å, r(H3–N) = 1.190 Å.
Electron density from the N–H3 bond is now concentrated
around the proton (dressed proton), represented by the V(H3)
basin with 0.48e, and at the new non-bonding valence basin
V_3(N) with 1.12e. In the valence shell of the N atom, two non-
bonding basins are now observed, V_2(N) and V_3(N). The
dressed proton is situated between two regions of the non-
bonding electron density, V_3(N) and V_1(O). It is worth
emphasising that hydrogen transfer occurs towards the lone pair
V_1(O) with 2.11e (in step VIII) that is observed from beginning
of the reaction. Topology of ELF in the step VIII also describes
the electronic structure of the transition state, TS3. The core and
valence attractors and ELF localisation domains are shown in
Fig. 7. Since the catastrophe is found before the TS3, it is
associated with no special event on the IRC path. Its electronic
structure corresponds to N–H bond breaking and creation of the
O–H bond. Electronic structure of TS3 is similar to the one
described for TS1, since both are characterised by partially
transferred H atom.

The next fold catastrophe (F), determines electronic
structure of the reacting system in the step IX. Further
shortening of the O···H3 distance and elongation of the
N···H3 distance is associated with electron density redistri-
bution from V_3(N) towards the V_2(N) basin, related to the
lone electron pair of the methanimine. Electron population
decrease in the V_3(N) basin results in electron localisation
changes and finally a catastrophe of the ELF field, ob-
served at R_x = 0.053 bohr. Other parameters at this point
are r(C–O) = 1.871 Å, r(O–H3) = 1.264 Å, r(H3–
N) = 1.283 Å. The V_3(N) attractor, its basin and associated
separatrix disappear. The number of core and valence
attractors reduces to 13. Basin population of the V_2(N),
calculated at the first point after the catastrophe, increases
to 3.44e. Since populations of other basins remain relative-
ly unchanged, the electron density from V_3(N) basin is
now 'contained' in the V_2(N) basin.

The final change of the electronic structure is observed in the
water fragment of the reacting system (step X). The shortening

Fig. 6 Evolution of the total
energy for the Schiff base
formation (reaction II) as a
function of the IRC coordinate
with marked positions of the
catastrophes on the ELF field
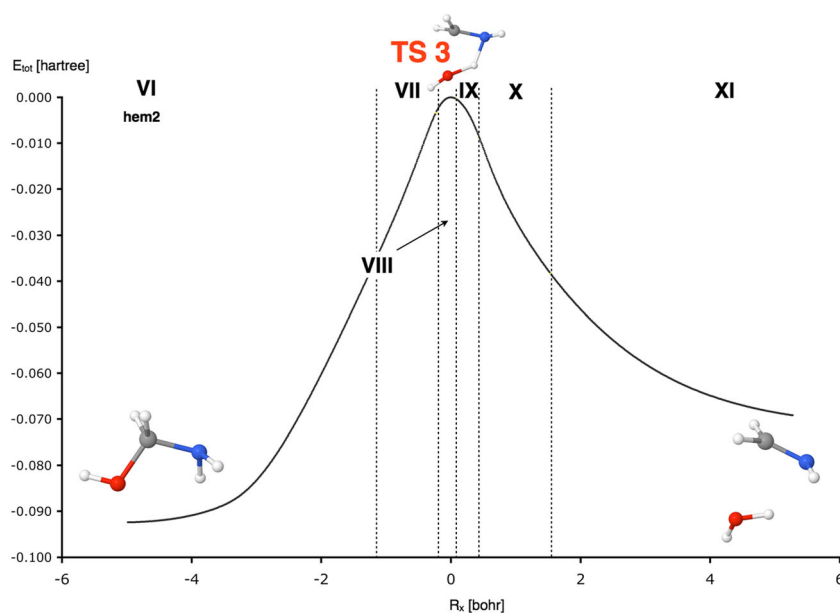
Fig. 7 The core and valence attractors and ELF localisation domains for the transition structure TS3 for the Schiff base formation reaction
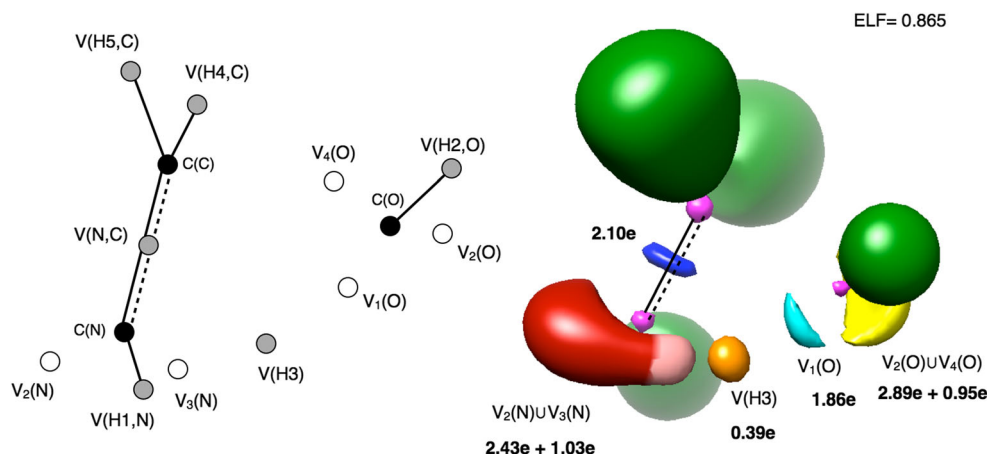
of the O··H3 distance and concentration of electron density in the region of the $V_2(O)$ basin (observed from step VI in hem2), associated with depopulation of the V(H3) basin (observed from the step VIII) leads to change in electron localisation in the O··H3 region and the next fold catastrophe (F). The catastrophe, observed for $R_x = 0.443$ bohr, corresponds to r(C–O) = 1.894 Å, r(O–H3) = 1.085 Å, r(H3–N) = 1.472 Å. The number of core and valence attractors is reduced to 12. The $V_1(O)$ attractor, its localisation basin, separatrix and critical point (3,−1) disappear and a wandering point (not CP) appears. The ELF function in the valence region of the H3–O bond is now characterised only by the protonated disynaptic attractor, V(H3,O). Post-fold basin population of V(H3,O) is 1.77e. From the ELF perspective, the H3–O bond has been formed and the water molecule established. The bonds and lone pairs represented by respective bonding and non-bonding basins are not yet fully saturated with the electron density. Final populations are established for the optimised geometrical structure of the last point on the IRC path.

In the last step of the reaction (XI), the topology of ELF function in the region of the N–C bond changes in the cusp catastrophe (C^+). The single attractor, V(N,C), characterising the covalent N–C bond in the steps VI–X (second reaction) and in the steps III–VI (first reaction), has been annihilated and two new attractors have appeared, $V_1(N,C)$ and $V_2(N,C)$. The total number of attractors increases to 13. The cusp has been found for $R_x = 1.528$ bohr, corresponding to r(C–O) = 2.030 Å, r(O–H3) = 0.979 Å, r(H3–N) = 1.831 Å. Local change of the ELF field is associated with concentration of the electron density in the N–C bond, shortened from 1.420 Å in the step VI ($R_x = −4.985$ bohr, first point on the IRC path going from TS3) to 1.278 Å in step X (the last point before the cusp). Corresponding value of $\overline{N}$ has increased from 1.77e to 2.67e. Since each $V_{i=1,2}(N,C)$ attractor can be associated with one formal bond in double bond in metanimine, it can be assumed (from ELF topological point of view) that a double N=C bond has been formed. However, it needs to be remembered that two $V_{i=1,2}(A,B)$ attractors are not always present for the double A=B bond, for example in the C=O bond. Two $V_{i=1,2}(C,C)$

attractors for formally double C=C bond have been first reported by Savin et al. [13] for ethylene. Silvi et al. [43] noted that localisation of two $V_{i=1,2}(A,B)$ attractors can be related to molecular symmetry instead of straightforward indication of a formally double bond. For two bonding disynaptic basins, $V_{i=1,2}(N,C)$, populations are 1.42 and 1.47e, respectively; thus, its sum is much smaller than 4e expected for the N=C bond. Further change of the molecular geometry results only in redistribution of the electron density among the basins. Population values of the $V_{i=1,2}(N,C)$ basins for the final point on the IRC path ($R_x = 5.249$ bohr) are 1.44 and 1.43e. Evolution of ELF field results shows therefore that water elimination from the hemiaminal and formation of Schiff base (methanimine) is complete. The reacting system now consists of the H_2O and H_2C=NH molecules. No other catastrophes of the ELF field have been found on the IRC path.

A final geometry optimisation of the reacting molecules yields the post-reaction complex H_2O··HN=CH_2, stabilised by the O–H··N hydrogen bond. Topological analysis of the $\rho(r)$ field confirms its existence via the presence of the (3,−1) critical point on the atomic interaction line, connecting the N atom and the hydrogen. The values of $\rho_{(3,-1)}(r) = 0.027$e/bohr³ and $\nabla^2 \rho_{(3,-1)}(r) = +0.085$e/bohr⁵ indicate a non-covalent interaction. Topology of ELF for the complex is the sum of the ELF topologies for the methanimine and water. A weak character of the interaction between H_2O and H_2C=NH molecules is demonstrated by similar values of $\overline{N}$ for the lone pairs in water and the isolated molecule.

The electronic structure of optimised isolated methanimine shows two bonding disynaptic basins, $V_{i=1,2}(N,C)$ for the N=C bond with 1.45 and 1.48e. Total population of the nitrogen-carbon bond is 2.93e. This value is smaller than 4e expected for the double bond and the 'missing' electron density can be found in two H–C bonds (2.12e) and the lone pair $V_2(N)$ on the nitrogen atom (2.68e). Analysis of the nitrogen-carbon bond polarity shows that the heteropolar nitrogen-carbon is polarised towards nitrogen. The value of the polarity index, p_{NC} is 0.36, and it is very similar to that of the formally single N–C bond in

the hem1 ($p_{NC} = 0.35$). The 1.99e comes from the N atom and 0.94e from the carbon atom. Nevertheless, both bonds are less heteropolar than the single C–O bond in the hem1 ($p_{OC} = 0.54$).

Comparison of the reaction mechanisms for hem1 and Schiff's base formation reveals some similarities. Topological analysis of ELF shows the same mechanism for hydrogen transfer in the N–H··O bridge. It consists of three main steps: breaking of the N–H bond, dressed proton transfer V(H) and formation of the O–H bond. The N–H bond breaking occurs very close to the respective TS for both reactions, i.e. for $R_x = - 0.073$ bohr (I reaction) and $R_x = - 0.189$ bohr (II reaction). Those correspond to the r(N–H) distance of 1.153 Å (I reaction) and 1.190 Å (II reaction), respectively. However, some interesting differences between both processes exist. For H transfer to occur in reaction I, presence of the non-bonding region of electron density, (the V(O) basin) is required. Its electron density forms the O–H bond, upon the end of the process. Such basin, V_3(O) is formed in step IV as a result the F^+ catastrophe. On the contrary, there is no need for the V(O) basin formation during the II reaction, since the existing lone pair basin, V_1(O), is used. The processes can be compared analysing steps IV, V and VI vs VIII, IX and X in Fig. 3.

Similarities can also be found, when analysing N–C bond formation in hem1 and C–O bond breaking in the formation of the Schiff base. Both processes exhibit very similar changes between the monosynaptic (no bonding) and disynaptic (bonding) basins. During the formation of the N–C bond, the monosynaptic basin V(N) changes to disynaptic V(N,C). For the dissociation of the C–O bond, a change of the disynaptic (bonding) V(C,O) to monosynaptic (no bonding) V(O) basin is observed.

Conclusions

Application of the Bonding Evolution Theory enabled a clear-cut description of the reaction mechanism between NH_3 and H_2CO, a useful prototype reaction for the formation of hemiaminal and Schiff base. This simple reaction serves as a basis for the analysis of more complicated reactions, leading to formation of stable hemiaminals involving for example triazole fragments. The study has been performed for two reactions: $H_2C=O + NH_3 \leftrightarrow$ hem1 and hem2 $\leftrightarrow HN=CH_2 + H_2O$. Comparison of the ELF topologies for two consecutive points on the IRC path enabled precise localisation of turning points (catastrophes), where the ELF topology of reacting molecules changes qualitatively. This helps to distinguish particular steps of the reaction, where covalent bonds are broken and/or formed.

The first reaction is the aminomethanol formation and consists of six steps (I–VI). Formation of methanimine (Schiff base) requires an additional six steps (VI–XI). The conformational change of the N–H bond and the oxygen lone pair in the hemiaminal does not change the topology of the ELF field.

Total number of steps in the $H_2C=O + NH_3 \leftrightarrow HN=CH_2 + H_2O$ reaction is 11.

Analysis of the BET results enables us to answer the questions posed in the Introduction as follows:

1. In order for the formation of hemaminal to happen, the nucleophillic attack of the nitrogen lone pair from NH_3 on carbon atom of H_2CO is required. This is followed by proton transfer in the N–H··O bridge. When the Schiff base is formed, the C–O bond is broken first, followed by proton transfer from the N–H bond to the O atom.

2. Formation of the N–C bond and the H atom transfer in the N–H··O bridge do not occur in TS1 and both processes do not occur simultaneously. Similarly, breaking of the C–O bond and the H atom transfer in the N–H··O bridge in the Schiff base formation do not occur in TS3. Breaking of the N–H bond occurs very close to the respective TS ($R_x < - 0.2$ bohr).

3. Mechanism of the simple $H_2CO + NH_3$ reaction is only partially similar to the mechanism generally proposed for the reaction between amine and aldehyde (Scheme 1). In the hemiaminal formation, firstly, the nucleophillic attack on the C atom in formaldehyde occurs, followed by the H atom transfer. However, the Schiff base is formed in a different way. The hydrogen transfer is preceded by the C–O bond breaking and the $[OH]^{\delta-}$ fragment detachment. Reaction mechanisms between formaldehyde and ammonia and benzaldehyde and 4-amine-4H-1,2,4-triazole triazole differ. The differences are clearly visible at the hemiaminal formation stage: the nucleophillic attack on the C atom precedes the hydrogen transfer, whereas for the triazole derivative reversed order is observed.

Compliance with ethical standards

References

1. Liebig J (1835) Über die Producte der Oxydation des Alkohols. Annalen der Pharmacie 14:133–167

2. Iwasawa T, Hooley RJ, Rebek Jr J (2007) Stabilization of labile carbonyl addition intermediates by a synthetic receptor. Science 317:493–496

3. Barys M, Ciunik Z, Drabent K, Kwiecien A (2010) Stable hemiaminals containing a triazole. New J Chem 34:2605–2611

4. Berski S, Ciunik L (2015) The mechanism of the formation of the hemiaminal and Schiff base from the benzaldehyde and triazole studied by means of the topological analysis of electron localization function and catastrophe theory. Mol Phys 113:765–781

5. Krokidis X, Noury S, Silvi B (1997) Characterization of elementary chemical processes by catastrophe theory. J Phys Chem A 101:7277–7282

6. Becke AD, Edgecombe KE (1990) A simple measure of electron localization in atomic and molecular systems. J Chern Phys 92:5397–5403

7. Silvi B, Savin A (1994) Classification of chemical bonds based on topological analysis of electron localization functions. Nature 371:683–686

8. Williams IH (1987) Theoretical modelling of specific solvation effects upon carbonyl addition. JACS 109:6299–6307

9. Hall NE, Smith BJ (1998) High-level ab initio molecular orbital calculations of imine formation. J Phys Chem A 102:4930–4938

10. Feldmann MT, Widicus SL, Blake GA, Kent DR, Goddard III WA (2005) Aminomethanol water elimination: theoretical examination. J Chem Phys 123:034304

11. Ding Y, Cui Y, Li T (2015) New views on the reaction of primary amine and aldehyde from DFT study. J Phys Chem A 119:4252–4256

12. Erdtman E, Bushnell EAC, Gauld JW, Eriksson LA (2011) Computational studies on Schiff-base formation: implications for the catalytic mechanism of porphobilinogen synthase. Comp Theor Chem 963:479–489

13. Savin A, Silvi B, Colonna F (1996) Topological analysis of the electron localization function applied to delocalized bonds. Can J Chem 74:1088–1096

14. Silvi B (2002) The synaptic order: a key concept to understand multicenter bonding. J Mol Struct 614:3–10

15. Savin A (2005) The electron localization function (ELF) and its relatives: interpretations and difficulties. J Mol Struct THEOCHEM 727:127–131

16. Savin A (2005) On the significance of ELF basins. J Chem Sci 117:473–475

17. Thom R (1972) Stabilité Structurelle et Morphogénèse. Intereditions, Paris,

18. Malcolm NOJ, Popelier PLA (2003) The full topology of the Laplacian of the electron density: Scrutinising a physical basis for the VSEPR model. Faraday Discuss 124:353–363

19. Zhao Y, Truhlar DG (2008) The M06 suite of density functionals for main group thermochemistry, thermochemical kinetics, noncovalent interactions, excited states, and transition elements: two new functionals and systematic testing of four M06-class functionals and 12 other functionals. Theor Chem Accounts 120:215–241

20. Frisch MJ, Pople JA, Binkley JS (1984) Self-consistent molecular orbital methods 25. Supplementary functions for Gaussian basis sets. J Chem Phys 80:3265–3269

21. Raghavachari K, Binkley JS, Seeger R, Pople JA (1980) Self-consistent molecular orbital methods. 20. Basis set for correlated wave-functions. J Chem Phys 72:650–654

22. Frisch MJ, Trucks GW, Schlegel HB, Scuseria GE, Robb MA, Cheeseman JR, Scalmani G, Barone V, Mennucci B, Petersson GA, Nakatsuji H, Caricato M, Li X, Hratchian HP, Izmaylov AF, Bloino J, Zheng G, Sonnenberg JL, Hada M, Ehara M, Toyota K, Fukuda R, Hasegawa J, Ishida M, Nakajima T, Honda Y, Kitao O, Nakai H, Vreven T, Montgomery Jr JA, Peralta JE, Ogliaro F, Bearpark M, Heyd JJ, Brothers E, Kudin KN, Staroverov VN, Keith T, Kobayashi R, Normand J, Raghavachari K, Rendell A, Burant JC, Iyengar SS, Tomasi J, Cossi M, Rega N, Millam JM, Klene M, Knox JE, Cross JB, Bakken V, Adamo C, Jaramillo J, Gomperts R, Stratmann RE, Yazyev O, Austin AJ, Cammi R, Pomelli C, Ochterski JW, Martin RL, Morokuma K, Zakrzewski VG, Voth GA, Salvador P, Dannenberg JJ, Dapprich S, Daniels AD, Farkas O, Foresman JB, Ortiz JV, Cioslowski J, Fox DJ (2013) GAUSSIAN 09, revision E.01. Gaussian, Inc., Wallingford,

23. Fukui K (1970) Formulation of the reaction coordinate. J Phys Chem 74:4161–4163

24. Fukui K (1981) The path of chemical reactions—the IRC approach. Acc Chem Res 14:363–368

25. Boys SF, Bernardi F (1970) The calculation of small molecular interactions by the differences of separate total energies. Some procedures with reduced errors. Mol Phys 19:553–566

26. AIMAll (Version 12.11.09), Todd A. Keith, TK Gr istmill Software, Overland Park KS, USA, 2012. http://aim.tkgristmill.com

27. Noury S, Krokidis X, Fuster F, Silvi B (1999) Computational tools for the electron localization function topological analysis. Comput Chem 23:597–604

28. Pettersen EF, Goddard TD, Huang CC, Couch GS, Greenblatt DM, Meng EC, Ferrin TE (2004) UCSF chimera—a visualization system for exploratory research and analysis. J Comput Chem 25:1605–1612

29. Krokidis X, Vuilleumier R, Borgis D, Silvi B (1999) A topological analysis of the proton transfer in $H_5O_2^+$. Mol Phys 96:265–273

30. Noury S, Silvi B, Gillespie RJ (2002) Chemical bonding in hypervalent molecules: is the octet rule relevant? Inorg Chem 41:2164–2172

31. Pilme J, Silvi B, Alikhani ME (2003) Structure and stability of M-CO, M = first-transition-row metal: an application of density functional theory and topological approaches. J Phys Chem A 107:4506–4514

32. Silvi B, Kryachko ES, Tishchenko O, Fuster F, Nguyen MT (2002) Key properties of monohalogen substituted phenols: interpretation in terms of the electron localization function. Mol Phys 100:1659–1675

33. Fourré I, Silvi B, Sevin A, Chevreau H (2002) Topological characterization of three-electron-bonded radical anions. J Phys Chem A 106:2561–2571

34. Polo V, Andres J, Castillo R, Berski S, Silvi B (2004) Understanding the molecular mechanism of the 1,3-dipolar cycloaddition between fulminic acid and acetylene in terms of the electron localization function and catastrophe theory. Chem - A Eur J 10:5165–5172

35. Alikhani ME, Fuster F, Silvi B (2005) What can tell the topological analysis of ELF on hydrogen bonding? Struct Chem 16:203–210

36. Krokidis X, Silvi B, Alikhani ME (1998) Topological characterization of the isomerization mechanisms in XNO (X=H, cl). Chem Phys Lett 292:35–45

37. Krokidis X, Goncalves V, Savin A, Silvi B (1998) How malonaldehyde bonds change during. Proton Transfer J Phys Chem A 102:5065–5073

38. Alikhani EM, Silvi B (2004) A topological analysis of the proton transfer in the HF- and HCl-(OH)⁻ interactions. J Mol Struct 706:3–6

39. Krokidis X, Silvi B, Dezarnaud-Dandine C, Sevin A (1998) Topological study, using a coupled ELF and catastrophe theory technique, of electron transfer in the li+Cl$_2$ system. New J Chem 22:1341–1350

40. Berski S, Andrés J, Silvi B, Domingo LR (2003) The joint use of catastrophe theory and electron localization function to characterize molecular mechanisms. A density functional study of the Diels-Alder reaction between ethylene and 1,3-butadiene. J Phys Chem A 107:6014–6024

41. Raub S, Jansen G (2001) A quantitative measure of bond polarity from the electron localization function and the theory of atoms in molecules. Theor Chem Accounts 106:223–232

42. Berski S, Durlak P (2016) The mechanism of Claisen rearrangement of allyl phenyl ether from the perspective of topological analysis of the ELF. New J Chem 40:8717–8726

43. Silvi B, Fourré I, Alikhani ME (2005) The topological analysis of the electron localisation function. A key for a position space representation of chemical bonds. Monatsh Chem 136:855–879